nuclear fusion
IAEA

PAPER • OPEN ACCESS

Suppression of anomalous impurity transport in NBI-heated W7-X plasmas

To cite this article: T. Romba *et al* 2023 *Nucl. Fusion* **63** 076023

View the article online for updates and enhancements.

You may also like

- A review of impurity transport characteristics in the LHD
Shigeru Sudo
- Observation of anomalous impurity transport during low-density experiments in W7-X with laser blow-off injections of iron
B. Geiger, Th. Wegner, C.D. Beidler et al.
- Investigation of oxygen impurity transport using the O^{4+} visible spectral line in the Aditya tokamak
M.B. Chowdhuri, J. Ghosh, S. Banerjee et al.

This content was downloaded from IP address 103.197.8.29 on 09/06/2023 at 07:28

OPEN ACCESS
IOP Publishing | International Atomic Energy Agency
Nuclear Fusion
Nucl. Fusion **63** (2023) 076023 (8pp)
https://doi.org/10.1088/1741-4326/acd5e1

Suppression of anomalous impurity transport in NBI-heated W7-X plasmas

T. Romba[1,*], F. Reimold[1], R.J.E. Jaspers[2], O.P. Ford[1], L. Vanó[1], T. Klinger[1] and the W7-X Team[a]

[1] Max-Planck-Institut für Plasmaphysik, Greifswald, 17491, Germany
[2] Eindhoven University of Technology, 5612 AZ Eindhoven, Netherlands

E-mail: thilo.romba@ipp.mpg.de

Received 10 January 2023, revised 3 April 2023
Accepted for publication 16 May 2023
Published 8 June 2023

Abstract

Radial impurity density profiles in two Wendelstein 7-X (W7-X) experiments heated by neutral beam injection (NBI) are analyzed with respect to their impurity transport properties. Local impurity densities are derived from charge exchange reactions with the W7-X NBI system using simulated neutral densities cross-validated with beam emission spectroscopy. Impurity profiles of argon and carbon are found to show an evolving central accumulation inside half radius. The properties of the underlying impurity transport are assessed using the one-dimensional transport code pySTRAHL. Comparisons between simulation and experiment indicate transport dominated by anomalous diffusion outside half radius. The observed central impurity accumulation is found to match best simulations with purely (neo-)classical transport in the accumulation region. This data implies a suppression of the anomalous impurity transport channel to below 35% of the (neo-)classical one. Experimental data is found to be matched best when invoking a time evolving, inward propagating zone where anomalous impurity transport is suppressed. An additional central power deposition into a plasma with central impurity accumulation via electron cyclotron resonance heating is found to affect the (neo-)classical transport components in case of operation times below 200 ms only. For longer operation times, it is found to re-introduce an altered level of anomalous diffusion. The existence of an inward directed anomalous pinch as an alternative explanation for the central impurity accumulation cannot explain the observed profiles.

Keywords: impurity transport, charge exchange recombination spectroscopy, Wendelstein 7-X

(Some figures may appear in colour only in the online journal)

1. Introduction

In a reactor plasma, the hydrogen isotopes deuterium and tritium serve as the fuel to the fusion reaction. Heavier atoms will be inherently present as well and are collectively referred to as impurities. Their sources range from the fusion reaction (He), over plasma wall interaction (Be, C, W), to gas seeding (N, Ne). While a certain amount of impurities can not be avoided or may even be desired, their presence, especially in the plasma core, puts at risk the self-sustained plasma burn. In a reactor, a reduction in fusion power by means of fuel dilution as well as increased radiative losses, especially in case of partially-ionized species, such as tungsten, restrict the permissible impurity amount strongly [1].

All impurities but helium are sourced outside the confined plasma region. They penetrate the plasma via particle transport perpendicular to the magnetic field lines. This radial

[a] See Sunn Pedersen *et al* 2022 (https://doi.org/10.1088/1741-4326/ac2cf5) for the W7-X Team.
[*] Author to whom any correspondence should be addressed.

Original Content from this work may be used under the terms of the Creative Commons Attribution 4.0 licence. Any further distribution of this work must maintain attribution to the author(s) and the title of the work, journal citation and DOI.

transport of impurities is composed of three distinct transport mechanisms. First, classical transport originates from collisions of unlike particles [2] and is small at high temperatures. In the cold plasma edge, this kind of transport becomes of importance [3]. Second, neoclassical particle transport stems from the collisions and drift orbits of particles due to the curvature and inhomogeneity of the magnetic field [4]. As a consequence from the three-dimensional magnetic field geometry, the ion and electron fluxes are not intrinsically ambipolar. This imbalance of radial currents gives rise to a radial electric field E_r, that drives strong neoclassical transport. In non-optimized stellarators, neoclassical transport is the dominant transport channel [5]. Classical and neoclassical transport is complemented by anomalous transport. This kind of transport originates from micro-instabilities that are driven most often by temperature and density gradient [2].

Independent of the transport channel, the particle transport in fusion devices is described by the 1D transport equation

$$\frac{\partial n_z}{\partial t} = -\nabla \cdot \vec{\Gamma}_z + S_z, \tag{1}$$

where n_z is the local impurity density in charge state z at time t, S_z are the sources and sinks of the respective charge state of the impurity, and $\vec{\Gamma}_z$ is the impurity flux. For edge sourced impurities, the source term vanishes inside the confined plasma region, leaving the impurity density in the core region governed by the radial impurity flux only. In cylindrical approximation, the radial component of the impurity flux is given by

$$[\nabla \cdot \vec{\Gamma}_z]_\rho = -\frac{1}{\rho}\frac{\partial}{\partial \rho}\rho\left(D\frac{\partial n_z}{\partial \rho} - V n_z\right) \tag{2}$$

where ρ is the normalized minor radius and D and V denote linearly scaling effective diffusion and convection coefficients. The different transport channels can be treated individually by separate diffusion and convection coefficients. The total transport being given by their sum. While V and D are calculated for the classical and neoclassical component, the anomalous transport component is typically inferred from matching experimental and simulated data sets accounting for the calculated contributions by an 'offset'.

The transport of particles is coupled to the transport of energy within the plasma. Due to this coupling, an optimization with respect to energy transport most often also reduces the particle transport within the plasma. The stellarator Wendelstein 7-X (W7-X) was optimized to fulfil MHD stability [6] and to exhibit reduced levels of neoclassical energy and particle transport [7]. The optimization with respect to the energy transport was found to be successful in [8]. As a consequence of the low neoclassical transport, the transport of impurities was found to be dominated by anomalous diffusion [9, 10] with no strong dependence on the elemental charge Z or mass m for low to high Z impurities [11, 12]. Heavy impurities are injected by laser-blow-off into plasmas heated by electron cyclotron resonance heating (ECRH). Measurements implied an anomalous diffusion of around 0.3 $m^2\,s^{-1}$ in the plasma core and up to 3 $m^2\,s^{-1}$ in the plasma edge [10].

The radial impurity profiles measured by charge exchange recombination spectroscopy (CXRS) in such plasmas are found to be flat. This implies low V/D [13]. In contrast, Vanó [14] report an accumulation of C^{6+} in the plasma core in scenarios heated by neutral beam injection (NBI). The observed local peaking in the impurity density implies $V/D \gg 1$, hinting at neoclassical transport characteristics. Their observation is qualitatively matched in transport simulations by a strong reduction of the anomalous transport component, allowing the inward directed neoclassical convection to accumulate impurities centrally. The main ion transport in this kind of discharges is found to be reduced to neoclassical levels transiently only [15].

The following work assesses such central impurity accumulation in NBI heated scenarios in W7-X with respect to the quantitative change in anomalous transport using simultaneous measurements of carbon and argon in case of two plasma discharges. The tools in use are discussed in section 2, the analysis of two plasma discharges with central impurity accumulation is done in section 3. Conclusions are drawn in section 4.

2. Methods

In the following, experimental anomalous diffusion and convection coefficients are inferred by matching time evolving experimental impurity density measurements to one-dimensional transport simulations of equation (1). The experimental local impurity densities are derived from CXRS [16]. The framework for the analysis is based on the neutral transport code pyFIDASIM [17]. It is discussed and validated in [13]. The correction to the argon rate data discussed by McDermott *et al* in [18] is transferred to the 436.52 nm transition line used in the following. As the injection energy of the W7-X neutral beam [19] is fixed during the experiment, the correction reduces to a rescaling of the rate data by a factor of 2.73 for all energy components.

Consistent with transport time scales, measured intensities are averaged over time intervals of 100 ms. Each active NBI source is simulated by pyFIDASIM using 20k markers.

Classical and neoclassical impurity transport coefficients are calculated. The contributions of the neoclassical transport coefficients L_{ii} can be separated in the diffusion convection framework into terms scaling with the local density gradient, D_z^{NC}, and the local density, v_z^{NC}, as:

$$\Gamma_z = -\underbrace{L_{11}^z}_{D_z^{NC}}\frac{\mathrm{d}n_z}{\mathrm{d}r} + \underbrace{\left[L_{11}^z\frac{q_z E_r}{T_z} - \left(L_{12}^z - \frac{3}{2}L_{11}^z\right)\frac{1}{T_z}\frac{\mathrm{d}T_z}{\mathrm{d}r}\right]}_{V_z^{NC}} n_z, \tag{3}$$

where $q_z = z \cdot e$ is the impurity charge, T_z is the impurity temperature set equal to the ion temperature, and L_{11}^z and L_{12}^z are

elements from the Onsager transport matrix [20]. Note that V_z^{NC} depends on D_z^{NC}, making the underlying dependencies complex. The neoclassical impurity transport coefficients used in the following are based on mono-energetic DKES calculations stored in an equilibrium specific data set [21, 22]. The mono-energetic transport coefficients are convoluted with a maxwellian characterising the local plasma parameters using the NEOTRANSP code [23]. NEOTRANSP is also used to calculate the classical contribution to the impurity transport based on the present plasma profiles. Both are calculated without enforcing momentum conservation, causing results in regions of high collisionality to be error-prone. In combination with the later imposed anomalous impurity transport profiles, the arising inaccuracies, primarily present in the plasma edge, do not fall into account in the conducted transport simulations.

Solutions to the 1D transport equation equation (1) are calculated using the pySTRAHL code [17, 24, 25]. In line with the averaging window of the experimental data, simulation parameters are adjusted in time increments of 100 ms.

3. Results

In the following, the impurity transport properties for two example cases for discharges exhibiting the impurity accumulation behaviour reported in [14] are assessed. The here presented trends are observed consistently for W7-X plasmas heated by NBI only [15]. The two discussed programs 20 181 009.016 and 20 181 009.034 represent a reference and an advanced scenario with good data availability, respectively.

Figure 1 depicts time traces of plasma parameters of the experiments. Both programs are performed in the high-mirror configuration of W7-X with an initial period of plasma heating by ECRH being followed by an NBI-heated phase. NBI sources 7 and 8 [19] were operated simultaneously with a total nominal NBI power of 3.5 MW. The pure NBI heating is accompanied by 100 ms of ECRH operation starting at 4.2 s with an averaged heating power of around 1.5 MW in program 20 181 009.016. In program 20 181 009.034, two seconds of pure NBI heating are followed by one second of simultaneous ECRH and NBI heating.

Radial profiles of plasma density, temperature, and (neo-)classical transport coefficients at three instances of program 20 181 009.016 are displayed in figure 2. Electron and ion temperature are found to be equal within the error bars of the profile diagnostics. For clarity, figure 2(*a*) depicts the ion temperature profile based on CXRS data only. The presented transport analysis is conducted with individual temperature profiles for electrons and ions.

In the course of the experiments, the central electron density and line averaged density (green dots and solid blue line in figure 1(*a*), respectively) are found to increase due to the central fueling by the NBI. From the radial density profiles in figure 2(*a*), it becomes apparent that this increase in density due to beam fueling is limited to the region of $\rho \leqslant 0.6$ with density profiles outside this radius remaining unchanged. Temperature profiles throughout the discharge are found to only change slightly. The ion and electron temperatures are found to be similar during NBI heating with profiles centrally peaking during added ECRH operation. Central ion temperature measurements by CXRS are complemented by XICS [26] in figure 1.

Figure 2(*b*) depicts the (neo-)classical transport coefficients for C^{6+} based on the profiles of figure 2(*a*). Due to the similar ion and electron temperatures, ion-root confinement is present, causing the convection to be directed radially inwards. The diffusion coefficient drops to zero at $\rho = 0$ due to a boundary condition in NEOTRANSP. At two instances, the contributions of the classical and neoclassical transport channels to V are indicated. While the convection in the initial phase is found to be primarily of neoclassical nature, at higher density both mechanisms contribute similarly. Note that V/D for the depicted data is of the order of -10, giving rise to a convection dominated (neo-)classical transport contribution.

Radial density profiles of argon and carbon at three exemplary points in time of program 20 181 009.016 are depicted in figure 3. As apparent from the profiles, the Ar^{16+} as well as the C^{6+} profiles are initially flat, consistent with the behaviour in ECRH discharges reported in [13]. The probed argon ionization state is found to be abundant only inside $\rho = 0.7$ due to the larger ionization energy compared to the everywhere abundant carbon state. All profiles within the first second of the discharge are found to be similar to the depicted gray data. In contrast, the subsequent profiles show a central peaking of the impurities inside half radius for both analysed species. The central impurity accumulation is consistent with the behaviour described in [14], hinting towards a significant reduction in the anomalous diffusion in the plasma core.

In the radial impurity profiles of figure 3, an impurity density gradient initially forms inboard of $\rho = 0.5$ with the profiles near the magnetic axis remaining initially flat (green data flat for low ρ). The local formation of an impurity density gradient implies significant convective transport ($V/D > 1$). In contrast, the locally flat profiles near the magnetic axis (green data for low ρ). This is consistent with small V/D. The clear difference in V/D across the profile indicates the presence of two regions with distinct transport characteristic inside $\rho = 0.5$. The central region of flat impurity density profiles is found to shrink over time, eventually leading to profiles fully peaked inside $\rho = 0.5$ (red data). Figure 4 shows measured experimental time traces of density densities at different radii (solid lines with error bars).

The central impurity accumulation is evident by the temporal increase in the central measurements only. Coinciding measured densities at different radii result from radially flat profiles in the given radial region in between the two different radial locations. The observation that densities at smaller radii coincide for longer is equivalent to the radial profiles remaining transiently flat near the magnetic axis. The points in time of program 016 at which two local density measurements start to deviate from another (dashed circles), show when local density gradient forms. The formation of local impurity density

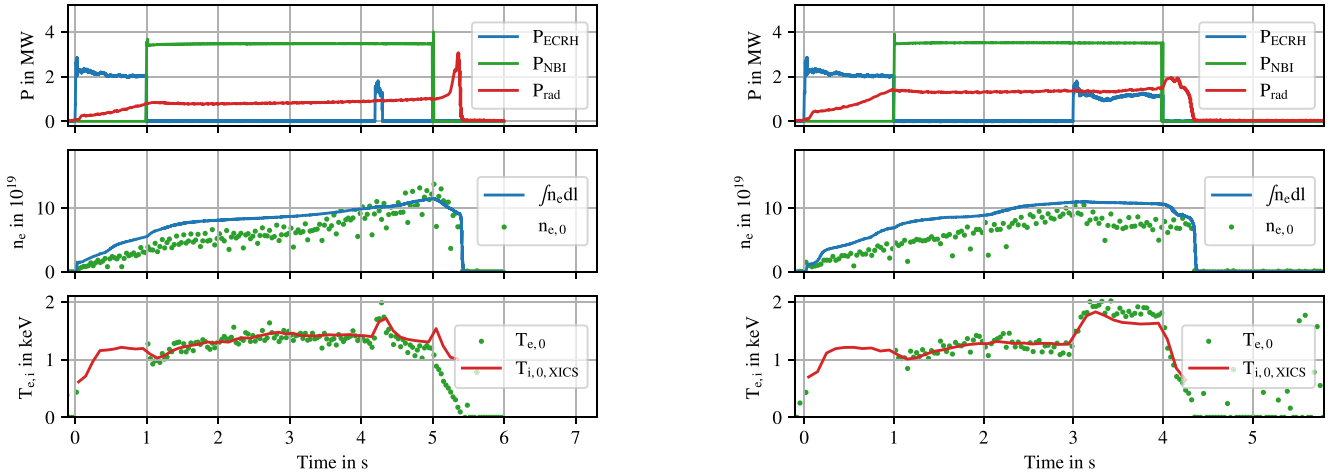

(a) Program 20181009.016

(b) Program 20181009.034

Figure 1. Overview over the central plasma parameters for the two analysed W7-X programs.

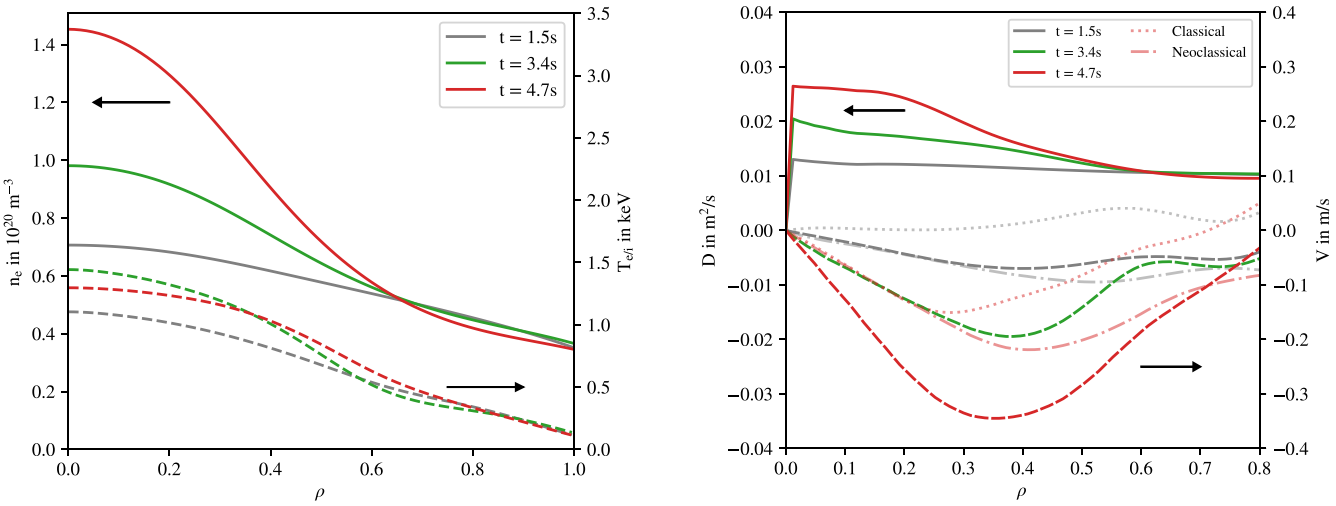

(a) Main plasma profiles

(b) (Neo-)classical transport coefficients for C^{6+}

Figure 2. Radial profiles of the main plasma parameters and the (neo-)classical transport coefficients at three points in time of program 20 181 009.016. For clarity, only T_i is plotted with T_e being similar within the errorbars of the profile diagnostics. The contributions of the classical and neoclassical transport channels for the convection velocity are indicated at two points in time.

gradients implies a significant increase in V/D. It is apparent that the region of large V/D extends further inwards over time, for both, argon and carbon, measurements. These marked time points of gradient formation are in the following referred to as 'separation events'.

In order to infer the impurity transport properties in this experiment, pySTRAHL simulations have been performed. The total convection velocity V is set to the sum of neoclassical and classical component. The diffusion coefficient is including neoclassical, classical, and an ad-hoc anomalous component, assessed in the following. The potential for the presence of an anomalous convective component is addressed later.

The results of these simulations at the respective radii accompany the experimental data in figure 4 (dashed lines). The simulation data is assigned with errors (shaded region) obtained by varying the radial location by 1 cm, to account for measurement uncertainties in the line of sight geometry.

The time dependent total diffusion coefficient for program 20 181 009.016 is shown in figure 5. Regions of low V/D (diffusion dominated) are identified by green color, those of high V/D in blue. As the radial profiles of figure 3 outside half radius are found to be flat, dominant anomalous diffusion of 0.1 $m^2\,s^{-1}$ is imposed in the region $\rho \geqslant 0.5$. Another, time varying, diffusion dominated region is introduced near the magnetic axis to account for the impurity density profiles being transiently flat near the magnetic axis. Based on the separation events of figure 4 (colored markers), the line of separation is chosen linear in ρ with time (dashed line joint fit to markers). Note that the extrapolation of the fit in the region of $\rho \leqslant 0.1$ is uncertain due to the lack of data points close to

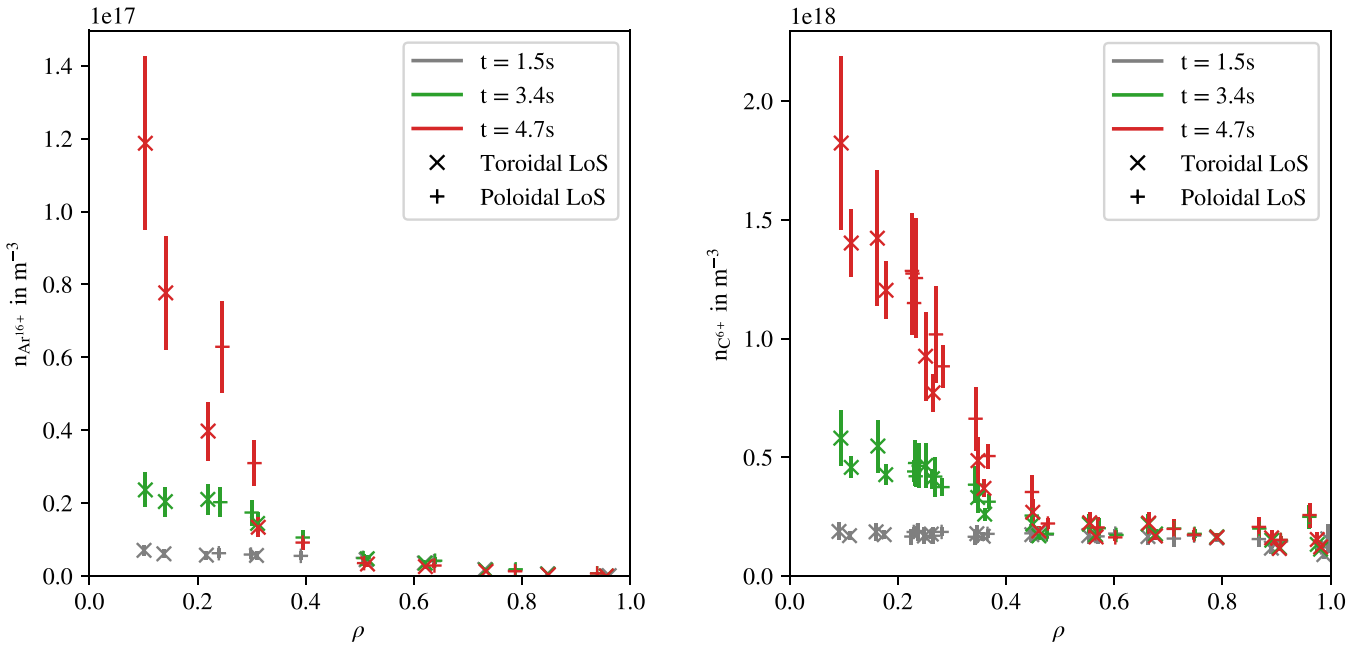

(a) Ar^{16+} densities (b) C^{6+} densities

Figure 3. Radial data points of argon and carbon at same three time points of program 20 181 009.016 as figure 2.

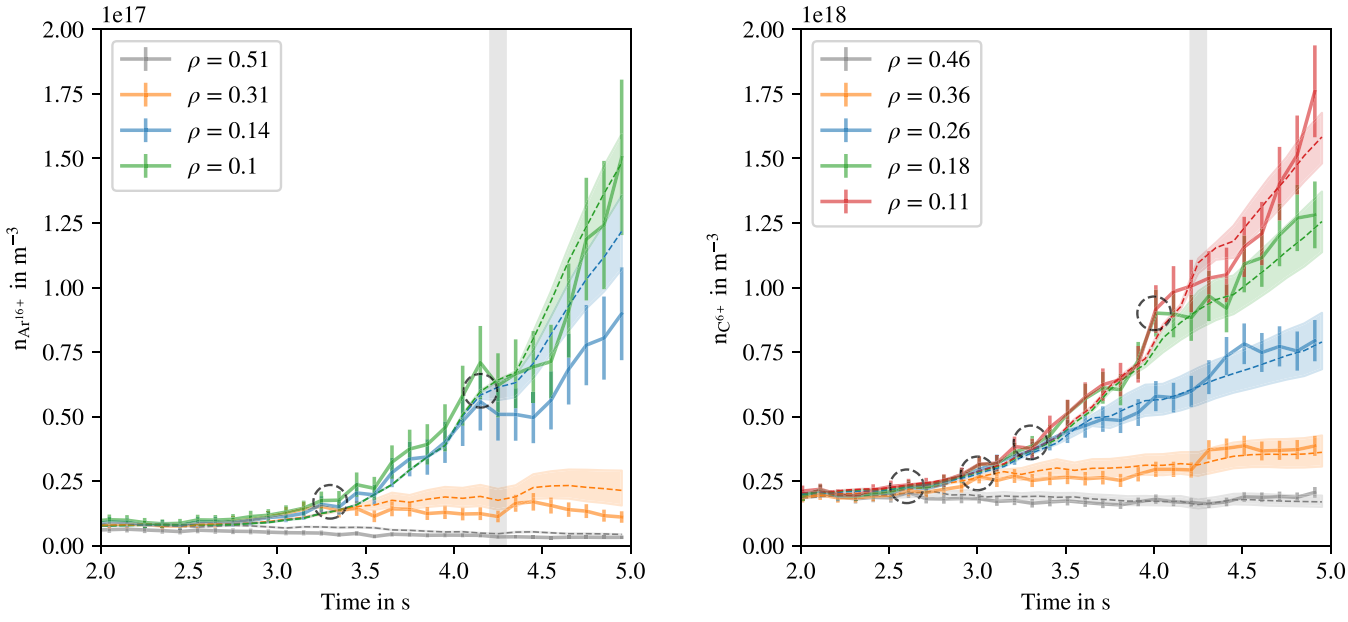

(a) Ar^{16+} densities (b) C^{6+} densities

Figure 4. Time traces of argon and carbon densities at different radial measurement locations of the toroidally oriented lines of sight of the W7-X CXRS system [27] for program 20 181 009.016. Error bars in the experimental data result from relative uncertainties in the simulated neutral densities, the fitted intensity, and the reaction rates. Intermittent ECRH operation of around 1.5 MW is indicated by the shaded region. Identified separation events are indicated by dashed black circles. Experimental data is complemented by pySTRAHL simulations at the respective radial locations indicated by dashed lines. Associated errors are indicated by shaded regions and obtained by a variation of the radial simulation location by 1 cm. Underlying is the diffusion of figure 5.

the magnetic axis. The green colored regions of small V/D are assigned with an anomalous diffusion of 0.1 $m^2\,s^{-1}$. This value corresponds to the lowest bound of the anomalous diffusion observed in ECRH programs which is found to range from 0.1 to 5.0 $m^2\,s^{-1}$ [13]. The diffusion in the blue shaded region is given by the sum of neoclassical and classical component only and is significantly below the imposed anomalous transport level.

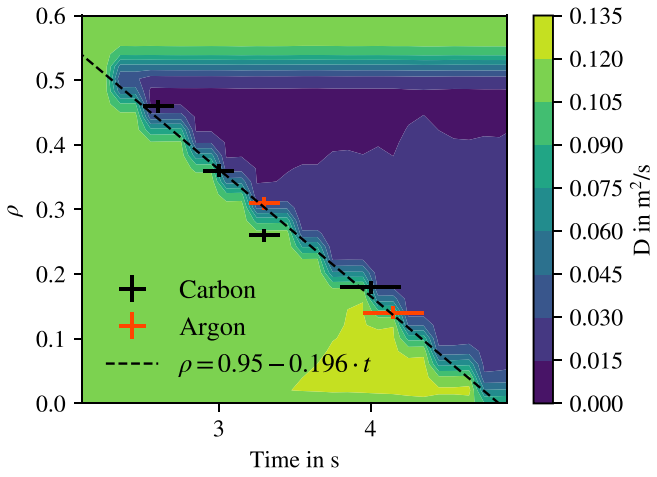

Figure 5. Time and ρ resolved plot of the total diffusion underlying the simulation of figure 4 for program 20 181 009.016. Regions of no anomalous diffusion are given by blue color with the residual diffusion being given by the sum of the classical and neoclassical components. Identified separation events are marked, a linear fit to these is given by the dashed line. Radial levels originate from the radial discretization into 27 locations.

The simulations of figure 4 match well with the experimental data and reproduce the gradual characteristic of the identified separation events. Reducing the anomalous diffusion inside $\rho = 0.5$ at once still allows a good match between experiment and simulation. However, the simulation is then unable to reproduce the consecutive gradient formation, i.e. it fails to reproduce a main observation in the measurements. While the experimental and simulated carbon data overlap within the given error bars throughout the whole discharge, the argon data shows an inferior match. This could be partly caused by the assumptions made within the DKES calculations not strictly applying in the collisionality regime of argon. Future works will have to compare to SFINCS [28] calculations which allow for higher collisionality regimes in the neoclassical transport calculations.

With the intermittent ECRH operation at 4.2 s, the argon accumulation stagnates momentarily while the carbon data shows no significant reaction. The stagnation of the central argon densities is also present in the simulated data with no anomalous diffusion being used. This implies that the change in transport via a neoclassical profile effect is sufficient to explain the experimentally observed behaviour rather than a transient occurrence of anomalous transport. The smaller reaction of the carbon to the profile changes is consistent with the expectation that neoclassical transport is exacerbated for higher Z impurities.

Based on the quantitative match between experiment and simulation with the anomalous transport being locally reduced to zero, it can be inferred that the anomalous diffusion component in this NBI-heated plasma is locally reduced to values below the sum of classical and neoclassical diffusion coefficient. With a neoclassical diffusion of the order of 0.02 $m^2\,s^{-1}$, the anomalous diffusion in such scenarios is reduced by a factor of more than ten relative to the lower bound found by CXRS in ECRH plasmas. As no saturation of the central data points is apparent in figure 4, the equilibrium of equation (1) set by the classical and neoclassical V and D is not reached after 4 s of NBI operation in the case at hand and the accumulation is progressing.

In the previously analyzed program 20 181 009.016, experimentally observed transport changes during short pulse operation of ECRH could be explained with changes of the neoclassical transport only. To assess the influence of continuous ECRH operation during impurity accumulation, figure 6 depicts carbon density time traces in case of the W7-X program 20 181 009.034. The discharge layout is given in figure 1(*b*) with NBI operation lasting for three seconds with ECRH being present throughout the whole last second of the discharge. The simulated time traces in figure 6 are obtained by setting the anomalous diffusion to 0.0 $m^2\,s^{-1}$ inside half radius starting with the first dashed vertical line. Note that such a simultaneous reduction of the anomalous diffusion inside half radius ignores the previously discussed separation events in the accumulation phase. During the accumulation phase a good qualitative match is obtained nonetheless.

In the experiment, the central impurity density is found to stagnate with the introduction of ECRH at 3.0 s. This stagnation is found to last for around 200 ms. During this phase, the simulated time traces match the experimental data well. Note that no anomalous diffusion is present in the simulation during this phase. This indicates that the stagnation of the central impurity relies on changes in the neoclassical transport coefficients only. The match between experiment and simulation thus indicates that the anomalous diffusion remains suppressed during the stagnation phase. This behaviour is expected to be equivalent to the previous observation in case of the ECRH blip of program 016.

The stagnation phase is followed by a phase of central flattening of the impurity profiles and a reduction of the accumulation. The densities in the central measurement volumes decrease and equilibrate with the gradient region moving radially outward. To match simulation and experiment, an anomalous diffusion of 0.02 $m^2\,s^{-1}$ is reintroduced at the second dashed line of figure 6. With neoclassical diffusion coefficients of around 0.015 $m^2\,s^{-1}$, the re-introduced anomalous diffusion is of neoclassical level. Note that during this flattening phase the measurements at smaller radii start to overlap earlier, i.e. profiles become initially flat near the magnetic axis. This observation is symmetric to the separation events in the accumulation phase. This may indicate that the reappearance of an anomalous diffusion initially takes place near the magnetic axis and subsequently propagates radially outwards.

The cause for the suppression of the anomalous impurity transport and the radial expansion of the suppression region is currently under investigation. The finite onset time of a reintroduction of an anomalous diffusion when adding ECRH to an impurity accumulated plasma in the analyzed discharges is found to correlate with the period in which the central electron and ion temperatures remain equal. A change of the neoclassical transport via ECRH induced changes in the temperature profiles is possible via L_{11}^z as well as the last term of equation (3), making the underlying actuators hard

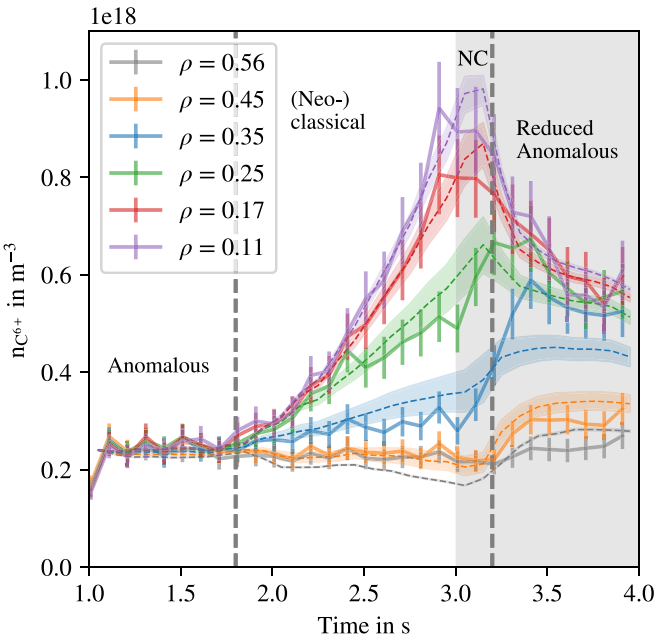

Figure 6. Measured and simulated time traces for W7-X program 20 181 009.034. Two seconds of pure NBI heating are followed by one second of simultaneous NBI and ECRH operation. The anomalous diffusion inside $\rho = 0.54$ in the simulation is reduced to 0.0 m^2 s^{-1} starting at the first dashed line and reintroduced with 0.02 m^2 s^{-1} inside same radius at the second dashed line. The ECRH operation phase is indicated by the shaded region.

to disentangle. As a central increase in the ion temperature alters the normalized temperature gradient, the balance within the convective terms may change, giving rise to the stagnation behaviour via neoclassical transport processes. In figure 1, the central electron and ion temperature are found to increase jointly during the stagnation phase. For longer operation times, the central ion temperature is found to drop below the electron one, in turn reducing the normalized temperature gradient. The re-introduction of anomalous transport is found to coincide with this decoupling. As the associated time scale matches typical energy confinement times in W7-X [29], the re-introduction of a reduced level of anomalous diffusion may be connected to a change in energy transport within the plasma.

So far, the experimentally observed impurity accumulation was shown to coincide with impurity transport reduced to (neo-)classical level. To estimate the potential of residual anomalous transport, the impurity transport simulations for program 20 181 009.016 were repeated with V and D increased by a joint scaling factor. As the (neo-)classical transport is fixed, this relates to an introduction of a residual anomalous transport component. V and D were scaled with the same factor to preserve the relative strength of convection and diffusion, in line with theoretical predictions [12].

It is found that simulations with increased impurity transport coefficients result in an acceleration in the impurity peaking trend. As the time evolution of the impurity densities was observed to be well matched in the purely (neo-)classical case of figure 4, this acceleration relates to a deterioration in the match between experimental and simulated time traces. Within the error bars of figure 4, simulations with residual anomalous transport up to 50% of the (neo-)classical one are contained. Due to the faster time dynamic, the simulated traces are found to lie in the upper bound of the experimental uncertainties however, giving rise to a systematically inferior match compared to the purely (neo-)classical case. This indicates that no strong anomalous impurity transport component is present during the observed peaking phase.

4. Summary

Radial density profiles of the impurities argon and carbon in NBI-heated W7-X plasmas have been analyzed with respect to their transport properties. After an initial period of radially flat profiles, the impurities are found to centrally accumulate inside half radius. By comparison with one-dimensional transport simulations, a localized, time-dependent suppression of anomalous transport of impurities was inferred. The region of suppressed impurity transport was confined to the region inside half radius and it is extent spread linearly in time from that radius inwards. Adding ECRH blips (<100 ms) during the accumulation phase altered the impurity transport via changed neoclassical transport coefficients. A reduced level of anomalous diffusion of order of the neoclassical component was required in case of continuous ECRH operation. The potential formation of an inward directed anomalous pinch setting the anomalous diffusion non-zero was assessed and found to be restricted to values of order $V_{\mathrm{anom}}/V_{\mathrm{NC}} < 0.5$. As a consequence, turbulence suppression of the impurity transport was found to be complete with allowable residual levels of order $D_{anom}/D_{NC} < 0.35$.

Acknowledgments

The authors give thanks to C Beidler for discussion of the neoclassical transport aspect and J M García Regaña for feedback on the manuscript.

This work has been carried out within the framework of the EUROfusion Consortium, funded by the European Union via the Euratom Research and Training Programme (Grant Agreement No. 101052200—EUROfusion). Views and opinions expressed are however those of the author(s) only and do not necessarily reflect those of the European Union or the European Commission. Neither the European Union nor the European Commission can be held responsible for them.

ORCID iDs

T. Romba https://orcid.org/0000-0002-2727-9385
F. Reimold https://orcid.org/0000-0003-4251-7924
R.J.E. Jaspers https://orcid.org/0000-0002-0589-7836
O.P. Ford https://orcid.org/0000-0002-5646-4758
L. Vanó https://orcid.org/0000-0001-7883-6471

References

[1] Pütterich T. 2005 Investigations of spectroscopic diagnostic of high-Z elements in fusion plasmas *PhD Thesis* Augsburg University

[2] Freidberg J.P. 2008 *Plasma Physics and Fusion Energy* (Cambridge: Cambridge University Press)

[3] Buller S., Mollén A., Newton S.L., Smith H.M. and Pusztai I. 2019 The importance of the classical channel in the impurity transport of optimized stellarators *J. Plasma Phys.* **85** 175850401

[4] Helander P. and Nührenberg J. 2009 Bootstrap current and neoclassical transport in quasi-isodynamic stellarators *Plasma Phys. Control. Fusion* **51** 055004

[5] Beidler C.D. *et al* 2011 Benchmarking of the mono-energetic transport coefficients-results from the international collaboration on neoclassical transport in stellarators (ICNTS) *Nucl. Fusion* **51** 076001

[6] Nührenberg J., Lotz W., Merkel P., Nührenberg C., Schwenn U., Strumberger E. and Hayashi T. 1995 Overview on Wendelstein 7-X theory *Fusion Technol.* **27** 71–78

[7] Erckmann V. *et al* 1997 The W7-X project: scientific basis and technical realization *17th IEEE/NPSS Symp. Fusion Engineering (Cat. No. 97CH36131)* vol 1 (IEEE) pp 40–48

[8] Beidler C.D. *et al* 2021 Demonstration of reduced neoclassical energy transport in Wendelstein 7-X *Nature* **596** 221–6

[9] Wegner T. *et al* 2020 Impact of the temperature ratio on turbulent impurity transport in Wendelstein 7-X *Nucl. Fusion* **60** 124004

[10] Geiger B. *et al* 2019 Observation of anomalous impurity transport during low-density experiments in W7-X with laser blow-off injections of iron *Nucl. Fusion* **59** 046009

[11] Langenberg A. *et al* 2020 Charge-state independent anomalous transport for a wide range of different impurity species observed at Wendelstein 7-X *Phys. Plasmas* **27** 052510

[12] García-Regaña J.M. *et al* 2021 Turbulent impurity transport simulations in Wendelstein 7-X plasmas *J. Plasma Phys.* **87** 855870103

[13] Romba T. *et al* 2022 Evaluation and validation of radial impurity density profiles from cxrs using neutral beam modelling in W7-X *Plasma Phys. Control. Fusion* (https://doi.org/10.1088/1361-6587/acd5c8)

[14] Vanó L. 2022 Carbon content and transport investigations on Wendelstein 7-X with charge exchange recombination spectroscopy *PhD Thesis* University of Greifswald

[15] Ford O.P. *et al* 2020 Turbulence reduced high performance scenarios in Wendelstein 7-X, on the path to a steady-state reactor *47th EPS Conf. on Plasma Physics*

[16] Fonck R.J., Darrow D.S. and Jaehnig K.P. 1984 Determination of plasma-ion velocity distribution via charge-exchange recombination spectroscopy *Physical Review A* **29** 3288–309

[17] Swee C., Geiger B., Dux R., Kumar S.T.A., Castillo J.F., Bader A. and Gerard M. 2021 Impurity transport studies at the HSX stellarator using active and passive CVI spectroscopy *Plasma Phys. Control. Fusion* **64** 015008

[18] McDermott R.M. Dux R., Guzman F., Pütterich T., Fischer R. and Kappatou A. 2020 Development of Ar^{16+} charge exchange recombination spectroscopy measurements at ASDEX Upgrade *Nucl. Fusion* **61** 016019

[19] Spanier A. *et al* 2021 Performance of the first neutral beam injector at the Wendelstein stellarator *Fusion Eng. Des.* **163** 112115

[20] Hirshman S.P. and Sigmar D.J. 1981 Neoclassical transport of impurities in tokamak plasmas *Nucl. Fusion* **21** 1079

[21] Hirshman S.P., Shaing K.C., Van Rij W.I., Beasley C.O. Jr and Crume E.C. Jr 1986 Plasma transport coefficients for nonsymmetric toroidal confinement systems *Phys. Fluids* **29** 2951–9

[22] Van Rij W.I. and Hirshman S.P. 1989 Variational bounds for transport coefficients in three-dimensional toroidal plasmas *Phys. Fluids* B **1** 563–9

[23] Smith H. 2022 NEOTRANSP (available at: https://gitlab.mpcdf.mpg.de/smithh/neotransp)

[24] Behringer K. 1987 Description of the impurity transport code 'STRAHL' *Technical Report* Commission of the European Communities

[25] Dux R. 2006 STRAHL User Manual 10/30 Max Planck Institute for Plasma Physics

[26] Pablant N.A. et al 2014 Measurement of core plasma temperature and rotation on W7-X made available by the x-ray imaging crystal spectrometer (xics) *Technical Report* Princeton Plasma Physics Lab.(PPPL), Princeton, NJ

[27] Ford O.P. *et al* 2020 Charge exchange recombination spectroscopy at Wendelstein 7-X *Rev. Sci. Instrum.* **91** 023507

[28] Landreman M., Smith H.M., Mollén A. and Helander P. 2014 Comparison of particle trajectories and collision operators for collisional transport in nonaxisymmetric plasmas *Phys. Plasmas* **21** 042503

[29] Fuchert G. *et al* 2018 Global energy confinement in the initial limiter configuration of Wendelstein 7-X *Nucl. Fusion* **58** 106029